

Adiabatic formulation of heteronuclear hydrogen molecular ion

B. D. Esry* and H. R. Sadeghpour†

Institute for Theoretical Atomic and Molecular Physics, Harvard-Smithsonian Center for Astrophysics, 60 Garden Street, Cambridge, Massachusetts 02138

(Received 18 March 1999; revised manuscript received 14 July 1999)

We revisit the HD^+ molecular ion by starting from a definition of the nonrelativistic adiabatic Hamiltonian that recovers the isotopic splitting. The Hamiltonian is written in prolate spheroidal coordinates with the origin at the nuclear center of mass. This prescription for the adiabatic Hamiltonian implicitly contains the symmetry-breaking effects arising from the mass difference between the proton and the deuteron, and gives the correct asymptotic atomic reduced masses. We calculate potential-energy curves, vibrational energies, transition dipole moments, and coupling matrix elements for HD^+ . In our adiabatic approximation, the isotopic splitting is recovered to nine significant digits at a value of $R=750a_0$. We investigate the dependence of the vibrational energies on the number of coupled electronic states, and compare with other calculations.

[S1050-2947(99)07311-4]

PACS number(s): 31.10.+z, 34.20.-b, 33.15.Fm, 33.20.Ea

I. BACKGROUND DISCUSSION

The Born-Oppenheimer (BO) Hamiltonian for the hydrogen molecular ion is one of the few Hamiltonians that separates in an orthogonal coordinate system. Due to this separability, H_2^+ and D_2^+ have been favorite molecules for detailed molecular structure calculations for nearly seven decades [1]. Nearly all structure properties of H_2^+ and D_2^+ , including electronic wave functions, rovibronic energies, hyperfine levels, electronic transition moments, and polarizabilities, can be calculated with spectroscopic precision.

Recent microwave measurements on H_2 Rydberg electrons in high angular momentum states have brought high-precision calculations of H_2^+ and D_2^+ into vogue [2,3]. Since the first nonmonopole term in the perturbative expansion of the Rydberg electron interaction with the ionic core is $\alpha/2r^4$, where r is the electronic coordinate, precise calculation of the core polarizability α is essential [2,4,5]. H_2^+ and D_2^+ do not possess permanent electric dipole moments. Hence electric dipole vibrational or rotational transitions in the infrared do not exist in H_2^+ and D_2^+ , and the spectroscopy is limited to the vacuum ultraviolet region.

Although HD^+ is an isotope of H_2^+ , it differs from its homonuclear brethren in several respects. While the BO Hamiltonian for HD^+ separates in prolate spheroidal coordinates (PSC's) just as for H_2^+ and D_2^+ , its symmetry under exchange of nuclei, *gerade* or *ungerade*, is broken owing to the mass difference between the proton and the deuteron. The so-called symmetry-breaking term in the HD^+ Hamiltonian couples the nuclear and electronic degrees of freedom, and gives rise to the splitting of the adiabatic potential-energy curves as the nuclei separate. An aspect of the mixing of the *gerade* and *ungerade* symmetries in HD^+ is that the

adiabatic potential-energy curves now nearly cross within each molecular symmetry, thereby inducing nonadiabatic transitions. (Potential curves of H_2^+ and D_2^+ exhibit real crossings.) Precisely for this reason, the lowest two adiabatic electronic curves in HD^+ couple, and, at energies slightly larger than 29 cm^{-1} , charge transfer can occur. For energies in the ‘‘mass gap,’’ the rovibronic levels in the $2p\sigma$ excited electronic curve are no longer true bound states, and fragment into a proton and a deuterium atom.

Although the electron in the $1s\sigma$ and $2p\sigma$ molecular orbitals of HD^+ tends to become localized on either the deuteron or the proton as the two nuclei separate, the energy separation of these two states affects the vibrational and rotational dynamics largely for energies near the dissociation limit. A far more profound influence on the physics of HD^+ occurs because the geometric center and the nuclear center of mass do not coincide. A permanent electric dipole is thus formed in the ground and excited electronic states, thereby giving HD^+ a vibration-rotation spectrum.

Aside from fundamental interest, studies of the $\text{H}^+ + \text{D}$ and $\text{D}^+ + \text{H}$ reactions are important in aeronomy and astrophysics. In planetary atmospheres, charge-exchange interactions between abundant isotopic hydrogen neutrals and ions regulate the neutral distribution and escape from the atmosphere [6]. The chemistry of deuterium in the postrecombination era of the early universe may depend on the charge transfer processes $\text{H}^+ + \text{D} \rightarrow \text{H} + \text{D}^+$ followed by $\text{H}_2 + \text{D}^+ \rightarrow \text{HD} + \text{H}^+$ [7]. The latter reaction is a major source of HD in diffuse interstellar clouds [8]. Determination of the D/H ratio also sets stringent constraints on models of big-bang nucleosynthesis [9,10].

Nearly all theoretical treatments of H_2^+ and its isotopes begin with a body-fixed coordinate system with the origin at the geometric center of the nuclei. Starting with the H_2^+ BO Hamiltonian in PSC's, electronic wave functions and energies are obtained as a function of the internuclear distance [11–13]. This definition of the BO Hamiltonian cannot, of course, discriminate between the two dissociation limits, $\text{H}^+ + \text{D}$ and $\text{D}^+ + \text{H}$. The *modus operandi* is to consider the symmetry-breaking term beyond the BO approximation. The

*Present address: J. R. Macdonald Laboratory, Dept. of Physics, Kansas State University, Manhattan, KS 66504. Electronic address: esry@phys.ksu.edu

†Electronic address: hsadeghpour@cfa.harvard.edu

mixing of the *gerade* and *ungerade* symmetries, within a degenerate perturbation expansion on the H_2^+ wave functions, is subsequently achieved by diagonalizing the symmetry-breaking operator, $-(1/2\mu_a)\nabla_r \cdot \nabla_R$, where $1/\mu_a = (1/m_H) - (1/m_D)$. In the variational-perturbation approach [12], the symmetry-breaking term is treated as a second-order perturbation to the standard adiabatic approximation, and bound vibrational energies with an accuracy of about 10^{-3} cm^{-1} are obtained. The variational approach of Bishop and Cheung [14] avoids the adiabatic approximation altogether, and instead obtains the eigenenergies of the full Hamiltonian by variational optimization of a trial wave function. A unitary transformation has also been used to [15–20] move the symmetry-breaking term from the kinetic-energy operator to the potential-energy operator as reduced-mass dependent effective charges on the nuclei, $z_1 \sim 1 - 1/4\mu_a$ and $z_2 \sim 1 + 1/4\mu_a$.

An alternative approach was proposed by Macek and Jerjian [21], who wrote the HD^+ Hamiltonian in mass-scaled hyperspherical coordinates (HSC's) and expanded the full wave function in the spirit of the BO approximation by treating the hyperradius as an adiabatic parameter. The HSC potential-energy curves that result for the two lowest states of HD^+ give the isotopically split dissociation limits, even in the lowest order of approximation. The reason for this can be traced to the fact that, as in all HSC calculations, the adiabatic Hamiltonian commutes with the kinematic rotation operators, ensuring that the adiabatic Hamiltonian is invariant under orthogonal coordinate transformations. In the usual BO approximation, the electron kinetic-energy operator, however, does not commute with the kinematic rotations, and thus gives incorrect limits for dissociation.

Tolstikhin *et al.* [22] introduced an alternative hyperspherical coordinate system, the hyperspherical elliptical coordinates, for the general three-body Coulomb problem that is especially well suited for the molecular problem. In fact, in the limit of infinitely heavy nuclei, these coordinates reduce to the usual prolate spheroidal coordinates. A somewhat more general three-body Hamiltonian was developed by Solov'ev and Vinitsky [23] in terms of the internuclear coordinate \mathbf{R} and the scaled electronic coordinate $\mathbf{r}' = \mathbf{r}/R$. They showed how to remove terms that couple electronic and nuclear motion by a transformation to a generalized adiabatic coordinate that depends explicitly on r' . It is worth noting that this slow coordinate is simply related to the hyperradius. Also, the Solov'ev-Vinitsky Hamiltonian yields our Hamiltonian if the origin of \mathbf{r}' is placed at the center of mass of the nuclei and it is written in terms of spheroidal coordinates.

Struensee *et al.* [24] diagonalized the HD^+ Hamiltonian in the center of mass of the nuclei, in a basis of body-fixed wave functions of definite angular momentum along the internuclear axis. These wave functions were constructed from a Slater orbital expansion to obtain adiabatic energy levels, transition energies, and dipole matrix elements.

In this work, we give an adiabatic formulation of HD^+ in PSC's that preserves the essential physics of the symmetry breaking. This physics is captured by including in the adiabatic Hamiltonian precisely the parts of the nuclear kinetic energy needed to give the correct asymptotic atomic reduced masses. We demonstrate numerically that the adiabatic po-

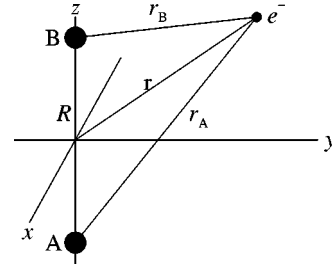


FIG. 1. The Jacobi set used in this work.

tential energies converge to the correct fragmentation thresholds. We present accurate calculations of the HD^+ potential-energy curves, coupling matrix elements, transition dipole matrix elements, vibrational energies, and transition frequencies. The chief advantages of this method are that we (a) recover the correct isotopic splitting in the adiabatic approximation, (b) calculate wave functions for nuclear motion that can be systematically improved, and (c) investigate effects beyond the adiabatic approximation for which we can calculate accurate coupling matrix elements. Here we limit ourselves to the determination of the vibrational energies. The scattering calculation using the potentials and couplings found here is in progress. We also present the dependence of the vibrational energies on the number of adiabatic channels. The energies obtained for a given number of channels are variationally stringent upper bounds to vibrational energies. In particular, this is true even for a one-channel calculation if the diagonal correction terms are included.

In an attempt to clarify possible ambiguities in terminology, we will define our use of the terms ‘‘BO approximation’’ and ‘‘adiabatic approximation.’’ By the BO approximation, we refer to the approximation in which the electronic Hamiltonian includes the electronic kinetic energy and the Coulomb interactions. The nuclear masses can either be taken to be infinite as is usually the practice, or they can be taken to be finite through their effect on the electronic reduced mass. The term adiabatic approximation will be reserved to label the more general approximation we develop here, in which some nuclear rotation and radial kinetic energy are included in the adiabatic Hamiltonian. Nonadiabatic effects can be taken into account in both approaches once the radial first and second derivatives are calculated.

II. THEORETICAL DISCUSSION

A. Adiabatic Hamiltonian construction

In this section, we present the adiabatic formulation for a general one-electron diatomic ion. In particular, for nuclei A and B with masses m_A and m_B , and charges Z_A and Z_B (see Fig. 1), we consider the nonrelativistic Hamiltonian in the center of mass:

$$H = -\frac{1}{2\mu_{AB}}\nabla_R^2 - \frac{1}{2\mu_e}\nabla_r^2 + \frac{Z_A Z_B}{R} - \frac{Z_A}{r_A} - \frac{Z_B}{r_B}. \quad (1)$$

This expression is written in atomic units (which will be used throughout this work), and the reduced masses are given by

$$\frac{1}{\mu_{AB}} = \frac{1}{m_A} + \frac{1}{m_B}$$

$$\frac{1}{\mu_e} = \frac{1}{m_A + m_B} + 1. \quad (2)$$

In considering the N -electron diatomic molecule, Pack and Hirschfelder [25] labeled these coordinates the center-of-mass nuclei system, since the origin of electronic coordinates is placed at the center-of-mass of the nuclei. But, for the one-electron case, this system of coordinates simply reduces to the Jacobi coordinates for the three-body system. The Jacobi coordinates, supplemented by the center-of-mass position in lab coordinates, are related by an orthogonal transformation to the lab coordinates of the particles. This leads to the absence of a mass polarization term in Eq. (1).

A main goal of the present development is to obtain the correct finite mass asymptotic thresholds in the zeroth order of approximation. In the case of HD^+ , this means that the $1s\sigma$ and $2p\sigma$ potential curves will be split by 29 cm^{-1} . To this end, our guiding principle in defining the adiabatic Hamiltonian will be to include as much of the full Hamiltonian [Eq. (1)], as possible, while retaining the internuclear distance R as the adiabatic parameter, i.e., retaining the concept of potential curves. This was also the approach taken by Pack and co-workers [24–26], although our implementation differs significantly from theirs. Our initial step, however, is identical to theirs. That is, we rewrite the nuclear orbital angular momentum \mathbf{L} in terms of the total orbital angular momentum \mathbf{J} , and the electronic orbital angular momentum \mathbf{l} . Explicitly, with $\mathbf{J} = \mathbf{L} + \mathbf{l}$, we have

$$\mathbf{L}^2 = \mathbf{J}^2 - 2J_z^2 + \mathbf{l}^2 - l_- J_+ - l_+ J_- . \quad (3)$$

The operators J_{\pm} and l_{\pm} are the usual angular momentum ladder operators for the total and electronic orbital angular momenta, respectively. Following the prescription of Pack and Hirschfelder [27] (save for the $R^{-5/2}$ factor), we expand the total internal wave function Ψ as

$$\Psi(\mathbf{R}, \mathbf{r}) = \sum_{\nu\Lambda} \frac{1}{R^{5/2}} F_{\nu}^{\Lambda}(R) \tilde{D}_{\Lambda M}^{(J)}(\phi, \theta, 0) \Phi_{\nu}^{\Lambda}(R; \mathbf{r}), \quad (4)$$

where θ and ϕ are the lab-fixed spherical polar coordinates of \mathbf{R} , and ν represents all of the quantum numbers needed to label the adiabatic channel functions Φ_{ν}^{Λ} (the purpose for using the $R^{-5/2}$ factor will become clear shortly). The tilde indicates that the Wigner D function is normalized over two angles rather than three, i.e., $\tilde{D}_{\Lambda M}^{(J)} = \sqrt{2J+1}/4\pi D_{\Lambda M}^{(J)}$ [26]. This expansion has the dual purpose of transforming the wave function to the body frame. (For comments on the subtleties of using the ladder operators in the body frame, see Pack and Hirschfelder [27] and Pack [26].)

We now reach the primary point of departure with the HD^+ development of Pack and co-workers [24,26]. Whereas they solved the adiabatic equation via an expansion over atomic orbitals, we write the electronic coordinates in terms of PSC's and solve the resulting two-dimensional (2D) equation using B splines (the details of the numerical treatment will be given in Sec. II B). Historically, PSC's have been

used for the homonuclear H_2^+ and D_2^+ systems because they allow the separation of the BO equations. The solutions are normally expanded in series and have been tabulated in the literature [28–30]. To the best of our knowledge, their use for heteronuclear systems has been limited to the generation of a BO basis which, in turn, is used to expand the electronic wave functions.

In the center-of-mass system, the PSC are defined just as in the geometric center of the nuclei (GCN) system:

$$\xi = \frac{r_A + r_B}{R}, \quad 1 \leq \xi < \infty,$$

$$\eta = \frac{r_A - r_B}{R}, \quad -1 \leq \eta < 1,$$

plus the azimuthal angle χ that ranges from 0 to 2π . The 6D volume element for the relative coordinates is

$$dV = R^5 (\xi^2 - \eta^2) d\xi d\eta d\chi \sin\theta dR d\theta d\phi, \quad (5)$$

and the electronic Laplacian has the usual prolate spheroidal definition

$$\nabla_r^2 = \frac{4}{R^2(\xi^2 - \eta^2)} \left[\frac{\partial}{\partial \xi} (\xi^2 - 1) \frac{\partial}{\partial \xi} + \frac{\partial}{\partial \eta} (1 - \eta^2) \frac{\partial}{\partial \eta} + \frac{\xi^2 - \eta^2}{(\xi^2 - 1)(1 - \eta^2)} \frac{\partial^2}{\partial \chi^2} \right].$$

Because the spheroidal coordinates depend on R , the effect on the nuclear radial derivatives of transforming to spheroidal coordinates must be considered. At this point, these derivatives are evaluated holding the body-frame Cartesian coordinates fixed. It is preferable, however, to evaluate them holding the spheroidal coordinates fixed instead. The consequence of working in the center-of-mass frame rather than in the GCN frame now appears since the only difference between the two coordinate systems is a translation in the Cartesian coordinate z ,

$$z_{\text{CMN}} = z_{\text{GCN}} + \frac{\alpha R}{2},$$

where α is the mass asymmetry parameter defined as

$$\alpha = \frac{m_A - m_B}{m_A + m_B}.$$

Thus, upon using the chain rule to rewrite the radial part of the nuclear Laplacian, we find

$$\left(\frac{\partial^2}{\partial R^2} + \frac{2}{R} \frac{\partial}{\partial R} \right)_{xyz} = \left(\frac{\partial^2}{\partial R^2} \right)_{\xi\eta\chi} - \left(\frac{2 \left(Y + \frac{3}{2} \right)}{R} \frac{\partial}{\partial R} \right)_{\xi\eta\chi} + \frac{\left(Y + \frac{3}{2} \right) \left(Y + \frac{5}{2} \right)}{R^2}, \quad (6)$$

keeping in mind that the radial derivatives are acting on the wave function in Eq. (4) and are taken holding $\xi\eta\chi$ fixed. The origin of the factor $R^{-5/2}$ in Eq. (4) is now evident—it prevents the first derivative on the left-hand side of Eq. (6) from appearing on the right-hand side, and it accounts for the R^5 in the volume element, Eq. (5). The operator Y in Eq. (6) involves only electronic coordinates and is defined as

$$Y = \frac{1}{\xi^2 - \eta^2} \left[(\xi + \alpha\eta)(\xi^2 - 1) \frac{\partial}{\partial \xi} + (\eta + \alpha\xi)(1 - \eta^2) \frac{\partial}{\partial \eta} \right].$$

For homonuclear systems, this definition corresponds precisely to the standard definition of Y [31], since the mass asymmetry parameter α is then zero.

To define the adiabatic Hamiltonian, we need only combine Eqs. (1), (3), and (6), while keeping R fixed. Care must be taken, however, as the last term in Eq. (6) is not Hermitian. Using the fact that

$$\left(Y + \frac{3}{2} \right)^\dagger = - \left(Y + \frac{3}{2} \right), \quad (7)$$

this term can be readily decomposed into its Hermitian and anti-Hermitian parts, and a Hermitian adiabatic Hamiltonian constructed. Finally, we have the following definition for the adiabatic Hamiltonian:

$$H_{\text{ad}} = -\frac{1}{2\mu_e} \nabla_r^2 - \frac{Z_A}{r_A} - \frac{Z_B}{r_B} + \frac{Z_A Z_B}{R} + \frac{J(J+1) - 2\Lambda^2 + \mathbf{I}^2}{2\mu_{AB}R^2} - \frac{\left(Y + \frac{3}{2} \right)^2}{2\mu_{AB}R^2}. \quad (8)$$

The full Hamiltonian in the CMN is thus given by

$$H = -\frac{1}{2\mu_{AB}} \frac{\partial^2}{\partial R^2} + \frac{Y + \frac{3}{2}}{\mu_{AB}R} \frac{\partial}{\partial R} - \frac{Y + \frac{3}{2}}{2\mu_{AB}R^2} - \frac{l_- J_+ + l_+ J_-}{2\mu_{AB}R^2} + H_{\text{ad}}.$$

In defining the adiabatic Hamiltonian we have chosen to include the term involving the angular momentum ladder operators—the Coriolis coupling term—in the full Hamiltonian rather than in the adiabatic Hamiltonian. From a purely fundamental point of view, however, it would be preferable to include this term in H_{ad} for two reasons. Including the Coriolis coupling term in H_{ad} would leave only radial kinetic energy out of the adiabatic diagonalization. In addition, the adiabatic potentials would themselves already show Λ doubling due to the electronic-rotation coupling. The drawback to this approach, however, is that the adiabatic Schrödinger equation becomes a system of $2J+1$ coupled equations that would have to be resolved for each value of the total angular momentum, J . This is, in fact, the prescription Struensee *et al.* followed in Ref. [24]. It yields accurate zeroth-order solutions, but it also limits the utility of an adiabatic approximation. Our choice of H_{ad} reduces the generation of (approximate) adiabatic potentials for arbitrary J to the simple addition of a centrifugal term to the $J=0$ curves. If spectroscopic accuracy for higher J 's is desired, the Cori-

olis coupling can be included once the matrix elements of the electronic orbital angular momentum ladder operators are known in the adiabatic channel function basis. For most other purposes, however, the simple addition of the centrifugal barrier suffices.

We note that the adiabatic Hamiltonian has the proper asymptotic properties; it gives the correct isotopic splitting and at $R \rightarrow \infty$, it yields the Jacobi reduced masses on each center, $\mu_A^{-1} = 1 + (1/m_A)$ and $\mu_B^{-1} = 1 + (1/m_B)$. For completeness, we now give the expression for the electronic orbital angular momentum in spheroidal coordinates. The most straightforward way to obtain this expression is to begin with the spherical polar coordinate form:

$$\mathbf{I}^2 = -\frac{1}{\sin \vartheta} \frac{\partial}{\partial \vartheta} \left(\sin \vartheta \frac{\partial}{\partial \vartheta} \right) - \frac{1}{\sin^2 \vartheta} \frac{\partial^2}{\partial \chi^2}. \quad (9)$$

Next, noting that

$$\sin \vartheta = \sqrt{\frac{(\xi^2 - 1)(1 - \eta^2)}{(\xi^2 - 1)(1 - \eta^2) + (\xi\eta + \alpha)^2}}$$

and

$$\frac{\partial}{\partial \vartheta} = \frac{\sqrt{(\xi^2 - 1)(1 - \eta^2)}}{\xi^2 - \eta^2} \left[(\eta + \alpha\xi) \frac{\partial}{\partial \xi} - (\xi + \alpha\eta) \frac{\partial}{\partial \eta} \right], \quad (10)$$

it is possible to evaluate \mathbf{I}^2 .

Given the adiabatic Hamiltonian [Eq. (8)], the channel functions and potentials are found by solving

$$H_{\text{ad}} \Phi_\nu^\Lambda(R; \mathbf{r}) = U_\nu^\Lambda(R) \Phi_\nu^\Lambda(R; \mathbf{r}). \quad (11)$$

Finally, the equations satisfied by the radial wave functions $F_\nu^\Lambda(R)$ from Eq. (4) are

$$\left[-\frac{1}{2\mu_{AB}} \frac{d^2}{dR^2} + U_\nu^\Lambda \right] F_\nu^\Lambda - \frac{1}{2\mu_{AB}} \sum_\lambda \left[2P_{\nu\lambda}^\Lambda \frac{d}{dR} + Q_{\nu\lambda}^\Lambda \right] F_\lambda^\Lambda - \frac{1}{2\mu_{AB}R^2} \sum_\lambda \left[\sqrt{J(J+1) - \Lambda(\Lambda+1)} C_{\nu\lambda}^{\Lambda-} F_\lambda^{\Lambda-1} + \sqrt{J(J+1) - \Lambda(\Lambda-1)} C_{\nu\lambda}^{\Lambda+} F_\lambda^{\Lambda+1} \right] = E F_\nu^\Lambda. \quad (12)$$

The coupling matrices \mathbf{P} and \mathbf{Q} in the above expression include the nonadiabatic effects resulting from the action of the nuclear radial derivatives on the channel functions. Explicitly,

$$P_{\nu\lambda}^\Lambda = \left\langle \Phi_\nu^\Lambda \left| \frac{\partial}{\partial R} - \frac{Y + \frac{3}{2}}{R} \right| \Phi_\lambda^\Lambda \right\rangle \quad (13)$$

and

$$Q_{\nu\lambda}^\Lambda = \left\langle \Phi_\nu^\Lambda \left| \frac{\partial^2}{\partial R^2} - \frac{2\left(Y + \frac{3}{2}\right)}{R} \frac{\partial}{\partial R} + \frac{Y + \frac{3}{2}}{R^2} \right| \Phi_\lambda^\Lambda \right\rangle, \quad (14)$$

and the Coriolis coupling matrix elements are

$$C_{\nu\lambda}^{\Lambda\pm} = \langle \Phi_{\nu}^{\Lambda\pm 1} | I_{\pm} | \Phi_{\lambda}^{\Lambda} \rangle.$$

It is immediately evident from the above expressions that the first- and second-order radial couplings $P_{\nu\lambda}^{\Lambda}$ and $Q_{\nu\lambda}^{\Lambda}$ are not the standard radial coupling matrix elements found in the literature. The added terms, which include the Y operator, ensure that Eq. (12) accounts for the full Hamiltonian. This division of terms results in an adiabatic Hamiltonian that correlates to hydrogenic thresholds with appropriate reduced masses, but introduces a term in the coupling matrix elements whose origin is the same as the so-called ‘‘translational factor’’ problem [23]. The asymptotic form of the second term in the first-order coupling matrix element in Eq. (13), $(Y + \frac{3}{2})$, behaves as R . This means that whereas the first term, $\partial/\partial R$, reaches infinity as $1/R$, the second term goes to a constant as R approaches infinity; this constant is proportional to $1/(1+m_A)$ [32].

For $J \neq 0$, \mathbf{P} and \mathbf{Q} retain their definitions in Eqs. (13) and (14) and still couple only those channels with the same Λ . The Coriolis coupling term, however, couples Λ and $\Lambda \pm 1$ channels— Σ and Π coupling in the case of $J=1$, for instance. Nonetheless, certain further approximations to Eq. (12) are useful. For instance, neglecting \mathbf{P} and \mathbf{Q} altogether decouples the adiabatic channels. The solution of the resulting single-channel equation for each channel gives the adiabatic vibrational energy levels. Including only the diagonal elements of \mathbf{Q} preserves the simple decoupled form, and yields upper bounds to the exact vibrational energies for the lowest channel. And, of course, by the variational principle, a truncation in the number of electronic states included in Eq. (12) also provides upper bounds to the exact vibrational energies for the lowest channel.

Even though we use PSC’s, the adiabatic Hamiltonian in Eq. (8) is nonseparable. The nuclear angular momentum and kinetic energy contributions (recall that the terms involving Y arose from the radial nuclear kinetic energy) to H_{ad} are nonseparable even in the homonuclear limit $\alpha=0$. Despite this nonseparability, the PSC’s are still well suited to this problem. Furthermore, the present adiabatic formulation can be useful even for the homonuclear problem. The advantage over the standard approach is that the potentials still go to the correct, finite mass separated-atom limit.

B. Numerical analysis

To obtain the channel functions and potentials, the adiabatic equation (11) must be solved. The χ dependence of the adiabatic wave function can be trivially separated, and a two dimensional equation in (ξ, η) remains. Thus, the simplification gained in having the best zeroth order adiabatic solutions is partially offset by the increased numerical complication of solving a two-dimensional partial differential equation. Such equations, however, can be handled readily on an average workstation using a convenient finite representation such as the discrete variable representation [33], finite elements [4,34], or B splines [35]. As stated above, we have chosen to use B splines for the present work.

B splines (or basis splines) are piecewise polynomials defined to have a finite extent on a grid. For example, a spline

constructed from k th-order polynomials in each grid interval spans $k+2$ grid points or $k+1$ intervals, and is zero outside of this region. Since they are splines, the coefficients of the polynomials are chosen to ensure continuous derivatives up to the k th derivative across each boundary between intervals, i.e., at the grid points. For the purposes of solving the adiabatic equation, the B splines can simply be regarded as a set of functions on which to expand the wave function. The channel function is thus written as

$$\Phi_{\nu}^{\Lambda}(R; \mathbf{r}) = \frac{e^{i\Lambda\chi}}{\sqrt{2\pi}} \sum_{m,n}^{M,N} c_{mn}^{(\nu)} u_m(\xi) v_n(\eta). \quad (15)$$

The wave function is characterized by the $M \times N$ expansion coefficients $c_{mn}^{(\nu)}$ describing its dependence on the sets of B spline functions $\{u_m\}$ and $\{v_n\}$. If N_{ξ} and N_{η} are the number of mesh points in each direction, then the upper limits of the sum in this expansion are determined by $M = N_{\xi} + k - 2$ and $N = N_{\eta} + k - 1$, where $k=5$ in the present calculations. These limits take into account the boundary conditions that Φ must be finite at $\xi=1$ and $\eta=\pm 1$, and that Φ vanishes at $\xi = \xi_{\text{max}}$.

Substituting $\Phi_{\nu}^{\Lambda}(R; \mathbf{r})$ from Eq. (15) into the adiabatic equation and projecting out $u_{m'}(\xi) v_{n'}(\eta)$ gives the matrix equation

$$\mathbf{H}_{\text{ad}} \mathbf{c}^{(\nu)} = U_{\nu}^{\Lambda}(R) \mathbf{S} \mathbf{c}^{(\nu)}. \quad (16)$$

The Hamiltonian matrix in the adiabatic approximation \mathbf{H}_{ad} is defined as [using the mapping $i = (n-1)M + m$]

$$(H_{\text{ad}})_{i'i} = \int d\xi \int d\eta (\xi^2 - \eta^2) \times u_{m'}(\xi) v_{n'}(\eta) H_{\text{ad}} u_m(\xi) v_n(\eta); \quad (17)$$

and the overlap matrix \mathbf{S} as

$$S_{i'i} = \int d\xi \int d\eta (\xi^2 - \eta^2) u_{m'}(\xi) v_{n'}(\eta) u_m(\xi) v_n(\eta). \quad (18)$$

Since these integrals must be evaluated numerically, it is advantageous to split the two-dimensional integrals into products of one-dimensional integrals wherever possible. The electronic kinetic energy, Coulomb potential energy, and overlap matrix elements all separate. For the terms arising from the nuclear rotation and kinetic energy, this separation is not possible, however, and two-dimensional integrations must be performed. All integrals are evaluated using Gauss-Legendre quadrature within each interval.

There is an additional manipulation that makes the numerical evaluation of these nonseparable integrals more stable and accurate. For both the electronic orbital angular momentum \mathbf{I}^2 and the $(Y + 3/2)^2$ term, the direct evaluation of the operator leads to problematic singularities at the nuclei, $(\xi, \eta) = (1, \pm 1)$. These singularities become less troublesome if use is made of the adjoint of the operator in question within the integral. For the \mathbf{I}^2 term, we rewrite the matrix element of the ϑ portion of Eq. (9) for arbitrary functions ψ and ϕ as

$$\begin{aligned} & \int_0^\pi d\vartheta \sin\vartheta \psi^* \frac{1}{\sin\vartheta} \frac{\partial}{\partial\vartheta} \left(\sin\vartheta \frac{\partial\phi}{\partial\vartheta} \right) \\ &= - \int_0^\pi d\vartheta \sin\vartheta \frac{\partial\psi^*}{\partial\vartheta} \frac{\partial\phi}{\partial\vartheta}. \end{aligned}$$

The electronic orbital angular momentum can now be readily evaluated within the prolate spheroidal B -spline basis using Eq. (10). For the $(Y+3/2)^2$ term, the approach is even simpler since the integral is initially written in PSC's. Using Eq. (7), we find

$$\begin{aligned} & \int_1^\infty \int_{-1}^1 d\xi d\eta (\xi^2 - \eta^2) \psi^* \left(Y + \frac{3}{2} \right)^2 \phi \\ &= - \int_1^\infty \int_{-1}^1 d\xi d\eta (\xi^2 - \eta^2) \left[\left(Y + \frac{3}{2} \right) \psi^* \right] \left[\left(Y + \frac{3}{2} \right) \phi \right]. \end{aligned}$$

The efficient numerical solution of Eq. (16) requires a knowledge of the structure of the Hamiltonian and overlap matrices. Because the B splines are strictly localized, the matrices \mathbf{H} and \mathbf{S} are banded. Banded matrices offer the benefit of reduced storage requirements compared to full matrices as well as more favorable scaling of the CPU time with the matrix dimension. Since each spline only overlaps the nearest k splines, the number of nonzero subdiagonals (or superdiagonals) is given for the present case by $N_\xi k + k + 1$. Note that this number would be $N_\eta k + k + 1$ had the mapping $i = (m-1)N + n$ been used for Eqs. (17) and (18) instead.

The benefits of the banded structure of the matrices in Eq. (16) can then be gained in the numerical solution of Eq. (16) through the use of routines from ARPACK [36]. ARPACK is a robust set of matrix eigenvalue routines based on a variant of the Lanczos algorithm [37] that are specifically designed for large sparse systems of equations.

The efficiency of the method is further improved if the (ξ, η) grid is optimized. Recalling that $\xi = (r_A + r_B)/R$, one immediate improvement can be made by setting the maximum value of ξ as

$$\xi_{\max} = \frac{R + r_0 + r_0}{R} = 1 + \frac{2r_0}{R},$$

where r_0 is chosen large enough that the wave function for the atomic state with the largest desired hydrogenic principal quantum number n fits within a distance r_0 from each center ($r_0 = 50$ a.u. in our calculations). The remaining optimization comes in choosing the grid point distribution. Even though the spheroidal coordinates largely handle the singularities at each nuclei, the additional measure of packing grid points near each center accounts for the fact that the wave functions become localized near the nuclear centers. In these calculations, we have chosen the ξ distribution to be $\xi_i = [\Delta_\xi(i-1)]^2 + 1$, $i = 1, \dots, N_\xi$, and the η distribution to be $\eta_i = -\cos[(i-1)\Delta_\eta\pi/2]$, $i = 1, \dots, N_\eta$. Using $\xi \in [1, \xi_{\max}]$ and $\eta \in [-1, 1]$, the grid spacing parameters Δ_ξ and Δ_η can be determined from the above expressions once N_ξ and N_η have been chosen. In the present calculations, $N_\xi = 60$ and $N_\eta = 120$.

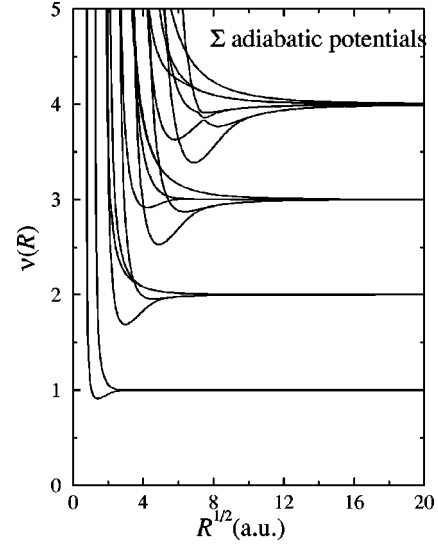


FIG. 2. The adiabatic potential-energy curves for the Σ symmetry. Only those potential curves converging to $n \leq 4$ hydrogenic thresholds are shown. Note that the horizontal axis has been scaled to the square root of the internuclear separation and that the vertical axis is given as the effective quantum number $\nu(R) = (-2U_\nu^0 \times(R))^{-1/2}$.

We also use B splines to solve the coupled radial equations [Eq. (12)]. The matrices are again banded, and the same numerical techniques can be used. The only specialization needed is for the grid point distribution. Our choice of $\lambda(R)/8$ for the radial grid spacing, with $\lambda(R)$ the local radial wavelength $2\pi/\sqrt{U_{1s\sigma}^0(\infty) - U_{1s\sigma}^0(R)}$, gives accurate results. Additional points must be added near avoided crossings, where radial derivative coupling elements are large, to represent rapid changes in the radial wave functions.

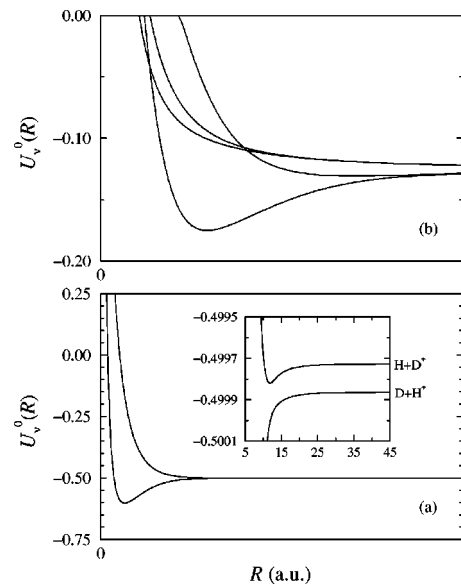


FIG. 3. (a) The $1s\sigma$ and $2p\sigma$ electronic adiabatic potential curves dissociating to $H^+ + D(1s)$ and $H(1s) + D^+$, respectively. The inset shows that the adiabatic Hamiltonian correctly recovers the splitting of the dissociation limits, and (b) the potential curves correlating to the first-excited states of hydrogen and deuterium.

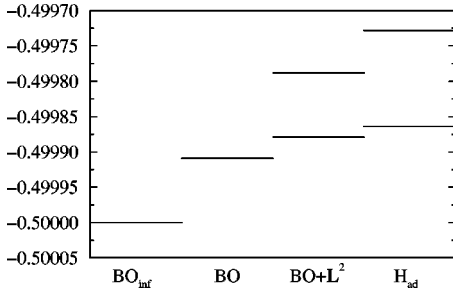


FIG. 4. The threshold energies (in a.u.) for the two lowest electronic states in HD⁺, in different levels of approximation. The calculated energies are at an internuclear distance of $R=750$ a.u.

III. RESULTS

In Fig. 2, we present our calculated adiabatic potential energy curves for HD⁺ for the Σ ($J=0$) symmetry. The conversion factors used in this work are as follows [38]:

$$\begin{aligned} m_D &= 3670.483014 \text{ a.u.}, \\ m_H &= 1836.152701 \text{ a.u.}, \\ 1 \text{ a.u.} &= 219474.6305 \text{ cm}^{-1}. \end{aligned}$$

The horizontal axis has been scaled to the square-root of the internuclear distance, and the vertical axis gives an effective quantum number, $\nu_\lambda(R) = (-2U_\lambda^0(R))^{-1/2}$. The 20 lowest HD⁺ potential curves are presented which correlate to hydrogenic dissociation thresholds up to $n=4$. In Fig. 3, we give the adiabatic potential energy curves which separate to H($n \leq 2$) and D($n \leq 2$) atomic levels. The inset in Fig. 3(a) shows the splitting of the electronic energies, due to the unequal masses of the proton and deuteron, as the molecules separate to two distinct dissociation limits. Because the sym-

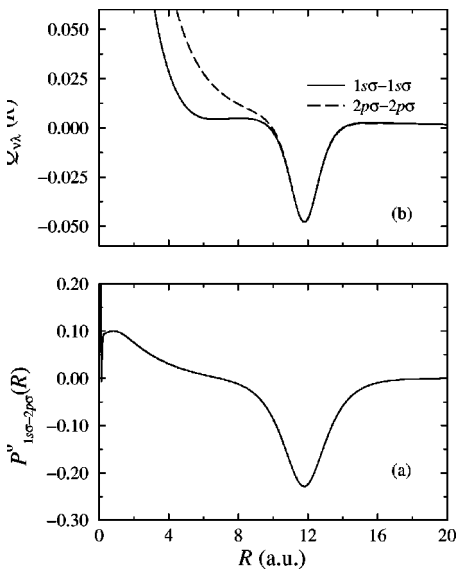


FIG. 5. (a) The radial coupling between the two lowest Σ electronic states of HD⁺. The profile is nearly Lorentzian near the avoided crossing at $R_0=12$ a.u., and, at small R , its behavior is dictated by the second anti-Hermitian term in Eq. (13). (b) The diagonal correction terms for the two lowest states.

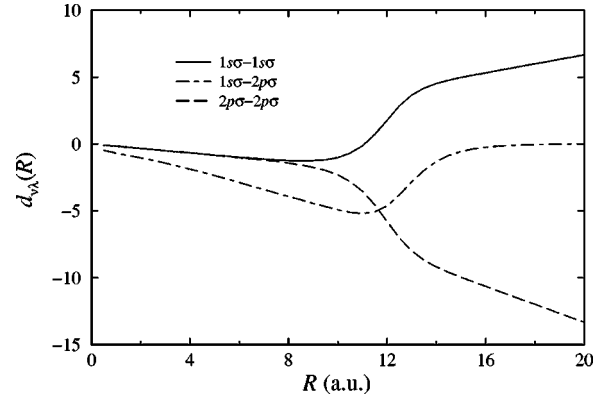


FIG. 6. The transition dipole moments between the $1s\sigma$ and $2p\sigma$ states in HD⁺. Only the electronic part of the dipole operator is shown. Note that the intrastate transition dipoles increase linearly with distance as the nuclei separate beyond the avoided crossing region at $R_0=12$ a.u. and the interstate transition dipole vanishes, as expected.

metry under the exchange of the two nuclei is broken, the adiabatic potential curves within each molecular symmetry exhibit avoided crossings, whereas the BO curves would show real crossings. The electronic curves which dissociate into H($n=2$)+D⁺ and D($n=2$)+H⁺ limits are given in Fig. 3(b). We note that these curves couple to each other and to other electronic potential energy curves.

In Fig. 4, the two lowest adiabatic potential energies for four different approximations are compared at $R=750$ a.u. The first is the infinite mass BO result in which both the D($1s$) and H($1s$) thresholds lie at -0.5 a.u. The second shows the effect of modifying the electron's reduced mass to reflect the finiteness of the nuclear masses, Eq. (2). This small change alone recovers a substantial fraction of the necessary shift, but the two thresholds remain degenerate. Once the effect of the nuclear orbital angular momentum is taken into account, indicated in the figure as BO+L², the thresholds are no longer degenerate, but still only about two-thirds of the full isotopic splitting is recovered. The final approximation is just Eq. (8) which goes beyond BO+L² by including a piece of the nuclear radial kinetic energy through $(Y+3/2)^2$. This approximation recovers the full isotopic splitting to nine significant digits already at this value of R (the

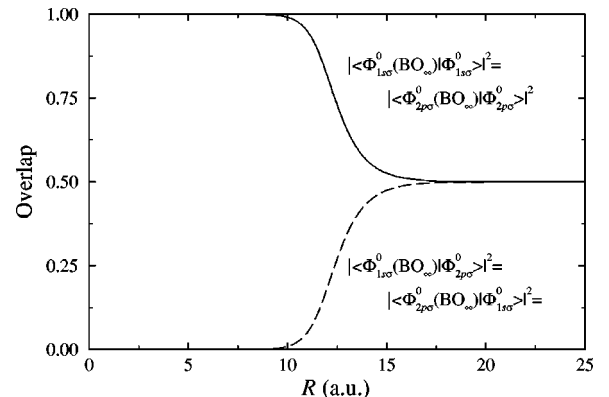


FIG. 7. The overlaps of the adiabatic wave functions for HD⁺ and the BO wave functions for H₂⁺ for the two lowest electronic states.

diagonal corrections contribute only 5.44×10^{-10} and 5.42×10^{-10} a.u., respectively). If we examined the diagonal corrections in either of the BO approximations or even the BO + \mathbf{L}^2 approximation, they would tend toward constants at large separations to make up for the inadequacy of the zeroth-order potentials. Furthermore, the off-diagonal \mathbf{P} matrix elements would also reflect this inadequacy, tending toward constants asymptotically for both the BO and BO + \mathbf{L}^2 approximations. While our formulation does not suffer from these same difficulties, it retains the small constant coupling described above. For bound vibrational state calculations, these ill-behaved coupling elements do not pose significant difficulties.

The radial coupling between the two lowest adiabatic potential curves, $1s\sigma$ and $2p\sigma$, is shown in Fig. 5(a). This coupling is localized around $R=12$ a.u., and its shape can, with good accuracy, be represented as

$$P_{1s\sigma-2p\sigma}^0(R) = -\frac{1}{2[(R-R_0)^2 + \Gamma^2/4]},$$

where $R_0=11.79$ a.u. and $\Gamma=2.97$ a.u. The small R behavior of $P_{1s\sigma-2p\sigma}^0(R)$ is governed by the second anti-Hermitian term in Eq. (13) which contributes to the non-Lorentzian profile. At very small R , the $2p\sigma$ curve has a narrow avoided crossing with a higher-lying curve that leads to an abrupt change of character in the coupling elements. In practice, the small- R behavior of the coupling matrix elements is of little consequence for spectroscopic and collision studies, however, as this behavior occurs in the classically forbidden region, where the radial wave functions have vanishing amplitudes. At large R , $P_{1s\sigma-2p\sigma}^0$ falls off exponentially, reflecting the decrease in overlap of the atomic wavefunctions on each center.

In Fig. 5(b), we present the diagonal correction terms, $Q_{1s\sigma-1s\sigma}^0(R)$ and $Q_{2p\sigma-2p\sigma}^0(R)$ from Eq. (14), as a function of R . Note that the diagonal correction terms can become positive, as the usual negative definite second-order radial derivative is augmented by the additional term, $-(Y+3/2)/R](\partial/\partial R)$ (the $Y+3/2$ term cannot contribute to diagonal elements of \mathbf{Q}). Asymptotically, both of these elements depend on R as R^{-2} to leading order. This result is another confirmation that the adiabatic potentials do, in fact, approach the exact atomic thresholds. If they did not, then the diagonal correction would approach a constant value asymptotically in order to produce the necessary shift in the potential to the correct threshold. This effect can be seen in Fig. 5(b) in the opposite R limit, the united-atom limit, in which the diagonal corrections from the present formulation are nonzero. This indicates that united atom limit is not correctly represented by the adiabatic channel functions calculated using Eq. (11).

The transition dipole matrix elements are shown in Fig. 6. The dipole matrix elements for parallel transitions are calculated as

$$d_{\nu\lambda}^A = -\alpha R - \langle \Phi_\nu^A | z_{\text{CMN}} | \Phi_\lambda^A \rangle,$$

where $z_{\text{CMN}}=(R/2)(\xi\eta+\alpha)$ in spheroidal coordinates. Figure 6 only shows the second term in the above equation. Near the united-atom limit, there is little dipole excitation as

the mass asymmetry is not evident to the electron. As the centers move away from each other, near the avoided crossing at $R_0=12$ a.u., the electric dipole begins to build up as the electron now ‘‘sees’’ two different centers. Once the nuclei have traversed the avoided crossing region, the dipole length increases fairly linearly with distance. The off-diagonal dipole matrix element that mediates transitions between the two electronic states vanishes at large separations as expected. In fact, it vanishes exponentially due to the reduction in overlap between the wave functions on each center.

The mass asymmetry manifests itself also in the overlaps between the two lowest electronic adiabatic wave functions $\Phi_{1s\sigma}^0$ and $\Phi_{2p\sigma}^0$, and their BO counterparts. These overlaps are plotted in Fig. 7 as a function of the internuclear distance. The interchannel and intrachannel overlaps begin, respectively, as 0 and 1, for appreciable distances between the centers. When the nuclei travel through the avoided crossing region, the character of the electronic wave functions in HD^+ change over a distance of about 3 a.u.; and for $R>20$ a.u., the overlaps approach each other and a near equal mixing of the BO wave functions results. This plot thus demonstrates the breakdown of the BO approximation: within the avoided crossing region, the channel functions show their molecular character and are well approximated by the BO functions; outside the avoided crossing, the channel functions become localized on one center or the other showing their atomic character.

The numerical values for the adiabatic $1s\sigma$ and $2p\sigma$ potential energies and all dipole matrix elements for parallel transitions among the two lowest electronic states are tabulated in Table I as a function of the internuclear distance. The calculations presented here are reported to a distance of $R=750$ a.u. We emphasize that as a consequence of our definition of the adiabatic Hamiltonian, the united-atom energy limit is not reproduced in our calculation. In Table II, we give the coupling matrix elements for the $1s\sigma$ and $2p\sigma$ electronic states of HD^+ in the range, $0 < R < 30$ a.u.

Table III gives the calculated $J=0$ and $\Lambda=0$ bound vibrational levels in cm^{-1} for states with primarily $1s\sigma$ character. We confirm that there are 23 bound vibrational levels and give upper bounds to the vibrational energies in the second column of Table III. The upper bounds are obtained when the diagonal correction terms are included in the calculation, and can be compared with the ‘‘improved adiabatic’’ results of Ref. [24] in column 7. The convergence of the energy levels with the number of adiabatic channels included in the coupled equations, Eq. (12), is illustrated in columns 3–6 of Table III. As expected, the dissociation energies increase as the number of coupled states is increased. In the final level of approximation, 20 adiabatic channels are included, encompassing all the states up to and including the $\text{H}(n=4)$ and $\text{D}(n=4)$ dissociation thresholds. Figure 8 gives a graphical demonstration of the behavior of a few selected vibrational energies as a function of the number of channels. The discrepancy with the results of the non-adiabatic calculation of Ref. [17], which are the best available calculations in the literature, is within a half wave number for the low vibrational levels and less than 0.1 cm^{-1} for the $\nu=21$ level. The variational-perturbation results of Ref. [12] are shown in column 8. For the last vibrational level,

TABLE I. Adiabatic potential energies and transition dipole matrix elements for the two lowest electronic curves in HD^+ as a function of the internuclear distance. Only the electronic part of the transition dipole operator is included.

R	$U_{1s\sigma}(R)$	$U_{2p\sigma}(R)$	$d_{1s\sigma-1s\sigma}(R)$	$d_{1s\sigma-2p\sigma}(R)$	$d_{2p\sigma-2p\sigma}(R)$
0.05	18.117649862	19.731159034	-0.00747	0.00120	0.00536
0.15	4.724966381	6.209944947	-0.02463	0.01262	0.07502
0.25	2.106852470	3.516798775	-0.04140	0.41370	0.02984
0.35	1.026217193	2.359702544	-0.05810	0.43847	-0.03736
0.45	0.456489700	1.715132871	-0.07477	0.46864	-0.06477
0.55	0.116721274	1.302177881	-0.09144	0.50242	-0.08574
0.65	-0.101348576	1.013167842	-0.10809	0.53875	-0.10457
0.75	-0.248161131	0.798033025	-0.12475	0.57680	-0.12246
0.85	-0.350267064	0.630404685	-0.14140	0.61589	-0.13988
0.95	-0.422884236	0.495147815	-0.15804	0.65546	-0.15704
1.05	-0.475301074	0.383015970	-0.17469	0.69504	-0.17404
1.15	-0.513467716	0.288085630	-0.19133	0.73431	-0.19094
1.25	-0.541344724	0.206412582	-0.20797	0.77308	-0.20777
1.35	-0.561651670	0.135279075	-0.22461	0.81127	-0.22456
1.45	-0.576304690	0.072750146	-0.24125	0.84888	-0.24132
1.55	-0.586683364	0.017402680	-0.25788	0.88600	-0.25806
1.65	-0.593799405	-0.031844039	-0.27452	0.92272	-0.27478
1.75	-0.598406563	-0.075836058	-0.29115	0.95919	-0.29150
1.80	-0.599952928	-0.096079395	-0.29946	0.97736	-0.29986
1.85	-0.601074134	-0.115254157	-0.30777	0.99552	-0.30821
1.90	-0.601820753	-0.133427031	-0.31609	1.01367	-0.31656
1.95	-0.602237240	-0.150659162	-0.32440	1.03183	-0.32492
2.00	-0.602362768	-0.167006838	-0.33271	1.05002	-0.33327
2.05	-0.602231928	-0.182522048	-0.34102	1.06825	-0.34162
2.10	-0.601875328	-0.197252966	-0.34933	1.08652	-0.34997
2.15	-0.601320101	-0.211244342	-0.35764	1.10486	-0.35833
2.20	-0.600590347	-0.224537843	-0.36595	1.12326	-0.36668
2.25	-0.599707504	-0.237172344	-0.37425	1.14174	-0.37503
2.30	-0.598690671	-0.249184173	-0.38256	1.16031	-0.38338
2.35	-0.597556890	-0.260607331	-0.39086	1.17898	-0.39174
2.40	-0.596321387	-0.271473683	-0.39916	1.19774	-0.40009
2.45	-0.594997780	-0.281813121	-0.40747	1.21662	-0.40845
2.50	-0.593598267	-0.291653719	-0.41577	1.23560	-0.41680
2.60	-0.590614122	-0.309942376	-0.43236	1.27394	-0.43352
2.70	-0.587443648	-0.326532589	-0.44896	1.31279	-0.45024
2.80	-0.584147142	-0.341595487	-0.46554	1.35218	-0.46697
2.90	-0.580773383	-0.355283193	-0.48212	1.39213	-0.48370
3.00	-0.577361880	-0.367731178	-0.49869	1.43267	-0.50044
3.20	-0.570547581	-0.389378478	-0.53180	1.51552	-0.53395
3.40	-0.563893534	-0.407358353	-0.56487	1.60079	-0.56750
3.60	-0.557522032	-0.422329400	-0.59789	1.68847	-0.60110
3.80	-0.551509634	-0.434822635	-0.63084	1.77850	-0.63477
4.00	-0.545901169	-0.445268253	-0.66372	1.87079	-0.66852
4.20	-0.540719139	-0.454016360	-0.69650	1.96520	-0.70236
4.40	-0.535970151	-0.461353122	-0.72916	2.06157	-0.73632
4.60	-0.531649421	-0.467513402	-0.76167	2.15972	-0.77043
4.80	-0.527744004	-0.472690701	-0.79401	2.25943	-0.80472
5.00	-0.524235177	-0.477045018	-0.82613	2.36049	-0.83922
5.20	-0.521100238	-0.480709087	-0.85799	2.46269	-0.87399
5.40	-0.518313912	-0.483793357	-0.88952	2.56582	-0.90909
5.60	-0.515849465	-0.486389989	-0.92066	2.66967	-0.94458
5.80	-0.513679596	-0.488576070	-0.95132	2.77406	-0.98055
6.00	-0.511777147	-0.490416218	-0.98138	2.87881	-1.01712

TABLE I. (*Continued.*)

R	$U_{1s\sigma}(R)$	$U_{2p\sigma}(R)$	$d_{1s\sigma-1s\sigma}(R)$	$d_{1s\sigma-2p\sigma}(R)$	$d_{2p\sigma-2p\sigma}(R)$
6.20	-0.510115668	-0.491964705	-1.01072	2.98380	-1.05441
6.40	-0.508669847	-0.493267184	-1.03917	3.08888	-1.09258
6.60	-0.507415820	-0.494362112	-1.06655	3.19396	-1.13184
6.80	-0.506331384	-0.495281920	-1.09260	3.29895	-1.17241
7.00	-0.505396119	-0.496053984	-1.11705	3.40378	-1.21459
7.20	-0.504591438	-0.496701423	-1.13953	3.50838	-1.25874
7.40	-0.503900575	-0.497243776	-1.15960	3.61272	-1.30530
7.60	-0.503308534	-0.497697557	-1.17674	3.71672	-1.35479
7.80	-0.502801995	-0.498076725	-1.19030	3.82035	-1.40786
8.00	-0.502369205	-0.498393079	-1.19948	3.92352	-1.46531
8.25	-0.501916348	-0.498715231	-1.20332	4.05169	-1.54475
8.50	-0.501545420	-0.498970842	-1.19646	4.17871	-1.63489
8.75	-0.501241937	-0.499172973	-1.17591	4.30411	-1.73872
9.00	-0.500993836	-0.499332176	-1.13788	4.42714	-1.86003
9.25	-0.500791127	-0.499456970	-1.07762	4.54658	-2.00358
9.75	-0.500490424	-0.499629432	-0.86556	4.76589	-2.38221
10.00	-0.500380144	-0.499687038	-0.69821	4.85802	-2.63284
10.25	-0.500290231	-0.499730571	-0.47794	4.92980	-2.93639
10.75	-0.500157564	-0.499786116	0.15553	4.96736	-3.73641
11.00	-0.500109423	-0.499802164	0.57701	4.90179	-4.24118
11.50	-0.500039512	-0.499818130	1.58497	4.51783	-5.41570
12.00	-0.499994884	-0.499819721	2.62286	3.77622	-6.62015
12.50	-0.499966321	-0.499813617	3.44540	2.85399	-7.60926
13.00	-0.499947250	-0.499804511	3.98942	2.00484	-8.31983
13.50	-0.499933621	-0.499795044	4.33920	1.35172	-8.83617
14.00	-0.499923243	-0.499786342	4.58756	0.89307	-9.25109
14.50	-0.499914976	-0.499778734	4.78964	0.58416	-9.61972
15.00	-0.499908201	-0.499772210	4.97178	0.38003	-9.96843
16.00	-0.499897788	-0.499761915	5.31577	0.15931	-10.64553
17.00	-0.499890272	-0.499754399	5.65259	0.06619	-11.31547
18.00	-0.499884717	-0.499748829	5.98796	0.02730	-11.98395
19.00	-0.499880536	-0.499744635	6.32288	0.01119	-12.65199
20.00	-0.499877341	-0.499741429	6.65755	0.00456	-13.31978
22.00	-0.499872924	-0.499736996	7.32641	0.00075	-14.65487
24.00	-0.499870153	-0.499734213	7.99480	0.00012	-15.98948
26.00	-0.499868345	-0.499732397	8.66285	0.00002	-17.32376
28.00	-0.499867127	-0.499731173	9.33066	0.00000	-18.65779
30.00	-0.499866283	-0.499730325	9.99829	0.00000	-19.99165
40.00	-0.499864512	-0.499728544	13.33492	0.00000	-26.65942
100.00	-0.499863808	-0.499727832	33.34391	0.00000	-66.65518
200.00	-0.499863809	-0.499727834	66.68861	0.00000	-133.31115
300.00	-0.499863812	-0.499727837	100.03304	0.00000	-199.96685
400.00	-0.499863813	-0.499727838	133.37743	0.00000	-266.62251
500.00	-0.499863814	-0.499727839	166.72181	0.00000	-333.27816
600.00	-0.499863814	-0.499727839	200.06618	0.00000	-399.93380
700.00	-0.499863815	-0.499727839	233.41054	0.00000	-466.58944
750.00	-0.499863815	-0.499727839	250.08273	0.00000	-499.91725

$\nu=22$, for which Refs. [17] and [12] do not report a number, the perturbation-variational result of Ref. [13] is used for comparison. Our calculation is more attractive by about 0.001 cm^{-1} .

We also calculate transition frequencies between dipole-allowed rovibronic energy levels in the $1s\sigma$ potential curve.

Table IV contains our calculated frequencies, neglecting relativistic and radiative effects, and the available observed transitions. Both the initial ($J=0$) and final ($J=1$) vibrational energy levels were calculated by coupling adiabatic channels up to $H(n=4)$ and $D(n=4)$ limits. The $J=1$ energies were approximated by retaining only the centrifugal

TABLE II. The nonadiabatic coupling and the diagonal corrections for the two lowest electronic curves in HD^+ as a function of the internuclear distance.

R	$P_{1s\sigma-2p\sigma}(R)$	$Q_{1s\sigma-1s\sigma}(R)$	$Q_{1s\sigma-2p\sigma}(R)$	$Q_{2p\sigma-1s\sigma}(R)$	$Q_{2p\sigma-2p\sigma}(R)$
0.05	2.06368	244.31070	-218.45547	-186.24894	313.47917
0.15	-0.00546	32.87653	-60.88075	-1.96632	82.92655
0.25	0.09223	12.19982	0.80822	-0.31699	18.21074
0.35	0.09523	6.32887	0.33243	0.24049	9.64447
0.45	0.09697	3.87200	0.24653	0.20843	5.85344
0.55	0.09834	2.61226	0.19190	0.16582	3.88919
0.65	0.09938	1.88004	0.15019	0.13260	2.74777
0.75	0.10002	1.41659	0.11607	0.10744	2.03105
0.85	0.10021	1.10456	0.08704	0.08817	1.55637
0.95	0.09989	0.88441	0.06194	0.07323	1.22999
1.05	0.09908	0.72326	0.04027	0.06151	0.99921
1.15	0.09778	0.60174	0.02182	0.05225	0.83209
1.25	0.09605	0.50782	0.00645	0.04492	0.70819
1.35	0.09396	0.43372	-0.00602	0.03909	0.61398
1.45	0.09156	0.37422	-0.01585	0.03444	0.54037
1.55	0.08895	0.32570	-0.02336	0.03074	0.48126
1.65	0.08617	0.28561	-0.02890	0.02778	0.43255
1.75	0.08330	0.25209	-0.03280	0.02541	0.39148
1.80	0.08184	0.23735	-0.03423	0.02440	0.37321
1.85	0.08037	0.22376	-0.03537	0.02350	0.35621
1.90	0.07889	0.21121	-0.03626	0.02270	0.34034
1.95	0.07742	0.19960	-0.03691	0.02197	0.32547
2.00	0.07595	0.18882	-0.03736	0.02132	0.31152
2.05	0.07449	0.17881	-0.03764	0.02073	0.29838
2.10	0.07303	0.16949	-0.03776	0.02020	0.28600
2.15	0.07159	0.16079	-0.03774	0.01973	0.27430
2.20	0.07016	0.15266	-0.03762	0.01930	0.26324
2.25	0.06875	0.14505	-0.03739	0.01891	0.25277
2.30	0.06735	0.13792	-0.03708	0.01855	0.24284
2.35	0.06596	0.13122	-0.03670	0.01824	0.23341
2.40	0.06460	0.12493	-0.03626	0.01795	0.22446
2.45	0.06325	0.11900	-0.03577	0.01768	0.21595
2.50	0.06193	0.11341	-0.03524	0.01744	0.20785
2.55	0.06062	0.10813	-0.03467	0.01722	0.20014
2.60	0.05933	0.10314	-0.03407	0.01702	0.19280
2.70	0.05682	0.09395	-0.03282	0.01666	0.17912
2.80	0.05438	0.08568	-0.03152	0.01636	0.16667
2.90	0.05203	0.07822	-0.03020	0.01610	0.15531
3.00	0.04975	0.07145	-0.02888	0.01587	0.14492
3.20	0.04543	0.05970	-0.02629	0.01547	0.12667
3.40	0.04140	0.04988	-0.02383	0.01513	0.11126
3.60	0.03763	0.04162	-0.02154	0.01480	0.09815
3.80	0.03412	0.03463	-0.01944	0.01448	0.08694
4.00	0.03084	0.02872	-0.01751	0.01414	0.07729
4.20	0.02778	0.02372	-0.01577	0.01377	0.06895
4.40	0.02493	0.01951	-0.01420	0.01338	0.06170
4.60	0.02226	0.01600	-0.01280	0.01297	0.05536
4.80	0.01977	0.01311	-0.01155	0.01253	0.04981
5.00	0.01744	0.01076	-0.01046	0.01208	0.04493
5.20	0.01526	0.00889	-0.00950	0.01164	0.04062
5.40	0.01321	0.00744	-0.00869	0.01120	0.03680
5.60	0.01127	0.00634	-0.00802	0.01080	0.03342
5.80	0.00944	0.00555	-0.00749	0.01044	0.03040
6.00	0.00768	0.00500	-0.00711	0.01015	0.02772

TABLE II. (Continued.)

R	$P_{1s\sigma-2p\sigma}(R)$	$Q_{1s\sigma-1s\sigma}(R)$	$Q_{1s\sigma-2p\sigma}(R)$	$Q_{2p\sigma-1s\sigma}(R)$	$Q_{2p\sigma-2p\sigma}(R)$
6.20	0.00598	0.00465	-0.00686	0.00993	0.02532
6.40	0.00431	0.00446	-0.00678	0.00983	0.02317
6.60	0.00265	0.00439	-0.00686	0.00985	0.02124
6.80	0.00096	0.00440	-0.00711	0.01003	0.01952
7.00	-0.00080	0.00446	-0.00757	0.01038	0.01796
7.20	-0.00265	0.00455	-0.00825	0.01095	0.01656
7.40	-0.00465	0.00465	-0.00918	0.01176	0.01529
7.60	-0.00686	0.00475	-0.01039	0.01285	0.01413
7.80	-0.00933	0.00482	-0.01194	0.01428	0.01308
8.00	-0.01213	0.00487	-0.01388	0.01610	0.01210
8.25	-0.01624	0.00486	-0.01694	0.01902	0.01096
8.50	-0.02120	0.00476	-0.02086	0.02281	0.00987
8.75	-0.02725	0.00451	-0.02583	0.02766	0.00878
9.00	-0.03468	0.00408	-0.03203	0.03375	0.00761
9.25	-0.04382	0.00335	-0.03966	0.04128	0.00626
9.75	-0.06881	0.00047	-0.05987	0.06131	0.00238
10.00	-0.08548	-0.00216	-0.07221	0.07357	-0.00065
10.25	-0.10531	-0.00602	-0.08510	0.08638	-0.00485
10.75	-0.15354	-0.01866	-0.10367	0.10480	-0.01806
11.00	-0.17951	-0.02740	-0.10136	0.10242	-0.02702
11.50	-0.22071	-0.04408	-0.05218	0.05304	-0.04407
12.00	-0.22435	-0.04591	0.03954	-0.03888	-0.04614
12.30	-0.20563	-0.03800	0.08257	-0.08204	-0.03832
12.35	-0.20139	-0.03630	0.08750	-0.08698	-0.03663
12.40	-0.19691	-0.03454	0.09201	-0.09152	-0.03488
12.45	-0.19223	-0.03275	0.09567	-0.09520	-0.03309
12.50	-0.18739	-0.03093	0.09867	-0.09821	-0.03129
12.55	-0.18240	-0.02911	0.10115	-0.10072	-0.02948
12.60	-0.17731	-0.02731	0.10287	-0.10245	-0.02768
12.65	-0.17215	-0.02553	0.10427	-0.10387	-0.02590
12.70	-0.16693	-0.02378	0.10500	-0.10462	-0.02416
12.75	-0.16169	-0.02209	0.10503	-0.10466	-0.02247
12.80	-0.15644	-0.02044	0.10502	-0.10467	-0.02083
12.90	-0.14603	-0.01735	0.10349	-0.10317	-0.01774
12.95	-0.14090	-0.01590	0.10218	-0.10187	-0.01629
13.00	-0.13584	-0.01452	0.10068	-0.10038	-0.01492
13.10	-0.12599	-0.01199	0.09681	-0.09654	-0.01239
13.20	-0.11654	-0.00975	0.09241	-0.09217	-0.01015
13.30	-0.10755	-0.00779	0.08744	-0.08722	-0.00818
13.50	-0.09112	-0.00462	0.07709	-0.07691	-0.00501
14.00	-0.05892	-0.00003	0.05261	-0.05249	-0.00039
14.50	-0.03748	0.00182	0.03428	-0.03421	0.00149
15.00	-0.02367	0.00247	0.02189	-0.02184	0.00217
16.00	-0.00935	0.00259	0.00817	-0.00815	0.00234
17.00	-0.00367	0.00237	0.00321	-0.00321	0.00217
18.00	-0.00143	0.00214	0.00126	-0.00126	0.00196
19.00	-0.00056	0.00193	0.00050	-0.00050	0.00178
20.00	-0.00022	0.00175	0.00019	-0.00019	0.00162
22.00	-0.00003	0.00145	0.00003	-0.00003	0.00136
24.00	-0.00001	0.00123	0.00000	0.00000	0.00116
26.00	0.00000	0.00105	0.00000	0.00000	0.00099
28.00	0.00000	0.00091	0.00000	0.00000	0.00086
30.00	0.00000	0.00080	0.00000	0.00000	0.00076

TABLE III. Dissociation energies of the vibrational levels in the $1s\sigma$ electronic potential curve as a function of the number of channels. The energies are given in cm^{-1} , and compared with the best calculations in the literature. In columns 3–6, our calculations include those electronic states leading up to each hydrogenic n manifold. The numbers in boldface represent our best results in Fig. 8.

ν	Dissociation energy (present)					Ref. [24]	Ref. [12]	Ref. [17]
	one-channel	two-channel ($n=1$)	six-channel ($n=2$)	12-channel ($n=3$)	20-channel ($n=4$)			
0	21515.928	21515.938	21515.975	21515.980	21515.981	21515.92	21516.071	21516.0096
1	19602.804	19602.834	19602.942	19602.956	19602.960	19602.80	19603.0741	19603.0382
2	17785.825	17785.872	17786.053	17786.076	17786.082	17785.82	17786.2133	17786.1989
3	16062.129	16062.191	16062.439	16062.470	16062.479	16062.12	16062.6261	16062.6309
4	14429.230	14429.304	14429.594	14429.635	14429.646	14429.22	14429.8263	14429.8484
5	12885.006	12885.091	12885.450	12885.499	12885.511	12885.00	12885.7018	12885.7300
6	11427.695	11427.789	11428.196	11428.253	11428.268	11427.68	11428.4710	11428.5124
7	10055.888	10055.989	10056.510	10056.574	10056.590	10055.88	10056.7373	10056.7886
8	8768.539	8768.645	8769.305	8769.378	8769.395	8768.53	8769.4502	8769.5098
9	7564.964	7565.073	7565.719	7565.799	7565.818	7564.96	7562.9269	7565.9926
10	6444.858	6444.969	6445.545	6445.622	6445.641	6444.85	6445.8606	6445.9306
11	5408.311	5408.421	5409.104	5409.186	5409.205	5408.30	5409.3399	5409.4124
12	4455.830	4455.938	4456.551	4456.643	4456.665	4455.82	4456.8696	4456.9446
13	3588.376	3588.479	3589.147	3589.250	3589.273	3588.36	3589.4114	3589.4847
14	2807.398	2807.495	2808.155	2808.233	2808.251	2807.39	2808.4084	2808.4802
15	2114.887	2114.975	2115.575	2115.658	2115.680	2114.87	2115.8512	2115.9191
16	1513.433	1513.511	1514.089	1514.159	1514.180	1513.42	1514.3266	1514.3886
17	1006.294	1006.360	1006.893	1006.959	1006.976	1006.28	1007.0888	1007.1436
18	597.449	597.503	597.946	597.996	598.010	597.43	598.1152	598.1587
19	291.566	291.622	291.950	291.986	291.997	291.55	292.0837	292.1173
20	93.442	93.779	93.973	93.995	94.001	93.55	94.0551	94.0754
21	9.033	10.159	10.201	10.210	10.215	8.76	10.2095	10.2140
22	0.323	0.425	0.429	0.430	0.431	0.32	0.430 ^a	

^aThe dissociation energy is taken from a calculation in Ref. [13].

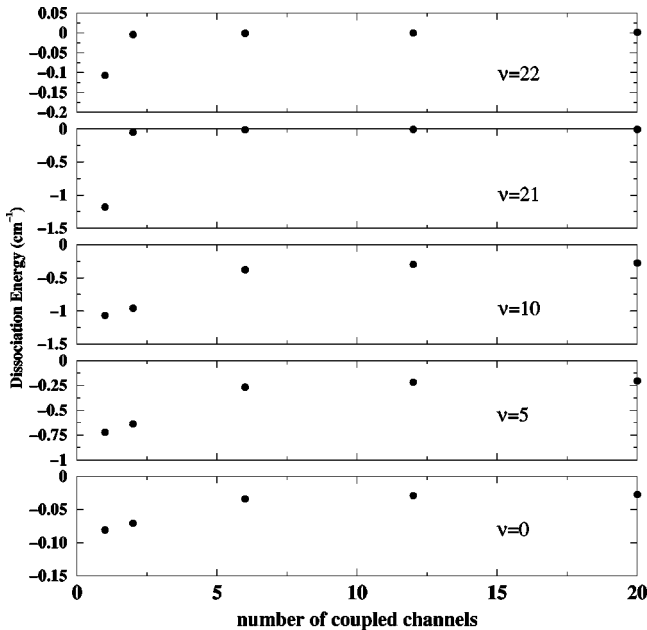


FIG. 8. The dissociation energies for selected vibrational levels (shown in boldface in Table III) in the $1s\sigma$ potential curve vs the number of electronic states. The zeros are taken to be the respective dissociation energies calculated in Refs. [18] and [14] for the last vibrational level.

term. Strictly speaking, one must include the Coriolis coupling terms in Eq. (12) to obtain an accurate measure of the final state energies.

IV. SUMMARY

In this work, an adiabatic reformulation of the HD^+ Hamiltonian that recovers the isotopic splitting of electronic states is presented in the prolate spheroidal coordinate system. The chief difference between our work and other for-

TABLE IV. Comparison of transition frequencies in cm^{-1} for the ground state of HD^+ . The difference between the calculated and observed transitions are given in column 4.

Transition	Calculated	Observed [1]	Difference
(1,0)–(0,1)	1869.159	1869.134	–.025
(2,1)–(1,0)	1856.796	1856.778	–.018
(17,1)–(14,0)	1813.814	1813.852	0.038
(18,1)–(16,0)	926.451	926.490	0.038
(20,0)–(17,1)	900.436	900.488	0.052
(20,1)–(17,0)	918.050	918.102	0.052
(21,0)–(17,1)	984.223	984.331	0.108
(22,1)–(17,0)	1006.860	1006.966	0.106

mulations of the HD^+ Hamiltonian is that we place the origin at the nuclear center of mass. This approach allows a more straightforward treatment in which the adiabatic potential-energy curves converge to the correct nonrelativistic fragmentation thresholds since they give the correct atomic reduced masses. Within this framework, we have evaluated the transition dipole matrix elements, radial couplings, vibrational energies, and transition frequencies, thereby providing for a unified treatment of bound and scattering processes. The numerical integrations are handled

with basis splines and the convergence of the vibrational energy levels with the number of electronic states is studied.

ACKNOWLEDGMENTS

This work was supported by a National Science Foundation grant to the Institute for Theoretical Atomic and Molecular Physics at the Harvard-Smithsonian Center for Astrophysics. B.D.E. acknowledges many fruitful discussions with I. Ben-Itzhak. We are grateful to M. Cavagnero for a critical reading of the manuscript.

-
- [1] A. Carrington, I. R. McNab, and C. A. Montgomery, *J. Phys. B* **22**, 3551 (1989).
- [2] Z. W. Fu, E. A. Hessels, and S. R. Lundeen, *Phys. Rev. A* **46**, R5313 (1992).
- [3] P. L. Jacobson, D. S. Fisher, C. W. Fehrenbach, W. G. Sturuss, and S. R. Lundeen, *Phys. Rev. A* **56**, R4361 (1997).
- [4] J. Shertzer and C. H. Greene, *Phys. Rev. A* **58**, 1082 (1998).
- [5] A. K. Bhatia and R. J. Drachman, *Phys. Rev. A* **59**, 205 (1999); J. M. Taylor, A. Dalgarno, and J. F. Babb, *ibid.* (to be published).
- [6] R. R. Hodges, Jr., *J. Geophys. Res.* **98**, 10 833 (1993).
- [7] P. C. Stancil, S. Lepp, and A. Dalgarno, *Astrophys. J.* **509**, 1 (1998).
- [8] A. Dalgarno, J. C. Weisheit, and J. H. Black, *Astrophys. J. Lett.* **14**, 77 (1973).
- [9] S. Burles and D. Tytler, *Astrophys. J.* **507**, 732 (1998).
- [10] A. A. Penzias, P. G. Wannier, R. W. Wilson, and R. A. Linke, *Astrophys. J.* **211**, 108 (1977).
- [11] A. Carrington and R. A. Kennedy, *Mol. Phys.* **56**, 935 (1985).
- [12] L. Wolniewicz and J. D. Poll, *J. Chem. Phys.* **73**, 8225 (1980); *Mol. Phys.* **59**, 953 (1986).
- [13] L. Wolniewicz and T. Orlikowski, *Mol. Phys.* **74**, 103 (1991).
- [14] D. M. Bishop and L. M. Cheung, *Phys. Rev. A* **16**, 640 (1977).
- [15] R. E. Moss, *J. Phys. B* **32**, L89 (1999).
- [16] R. E. Moss and I. A. Sadler, *Mol. Phys.* **66**, 591 (1989).
- [17] G. G. Balint-Kurti, R. E. Moss, I. A. Sadler, and M. Shapiro, *Phys. Rev. A* **41**, 4913 (1990).
- [18] R. E. Moss and I. A. Sadler, *Mol. Phys.* **61**, 905 (1987).
- [19] W. R. Thorson, J. H. Choi, and S. K. Knudson, *Phys. Rev. A* **31**, 22 (1985); **31**, 34 (1985).
- [20] A. V. Matveenko, *Phys. Lett.* **129**, 11 (1983).
- [21] J. Macek and K. A. Jerjian, *Phys. Rev. A* **33**, 233 (1986).
- [22] O. I. Tolstikhin, S. Watanabe, and M. Matsuzawa, *Phys. Rev. Lett.* **74**, 3573 (1995).
- [23] E. A. Soloviev and S. I. Vinitsky, *J. Phys. B* **18**, L557 (1985).
- [24] M. C. Struensee, J. S. Cohen, and R. T. Pack, *Phys. Rev. A* **34**, 3605 (1986).
- [25] R. T. Pack and J. O. Hirschfelder, *J. Chem. Phys.* **52**, 521 (1970).
- [26] R. T. Pack, *Phys. Rev. A* **32**, 2022 (1985).
- [27] R. T. Pack and J. O. Hirschfelder, *J. Chem. Phys.* **49**, 4009 (1968).
- [28] G. Jaffe, *Z. Phys.* **87**, 535 (1934).
- [29] E. A. Hylleraas, *Z. Phys.* **71**, 739 (1931).
- [30] D. R. Bates, K. Ledsham, and A. L. Stewart, *Philos. Trans. R. Soc. London, Ser. A* **246**, 215 (1953).
- [31] A. Carrington and R. A. Kennedy, in *Gas Phase Ion Chemistry Vol. 3: Ion and Light*, edited by M. T. Bowers (Academic, London, 1984).
- [32] B. D. Esry (unpublished).
- [33] J. C. Light, I. P. Hamilton, and J. V. Lill, *J. Chem. Phys.* **82**, 1400 (1985).
- [34] B. D. Esry, C. D. Lin, and C. H. Greene, *Phys. Rev. A* **54**, 394 (1996).
- [35] C. de Boor, *A Practical Guide to Splines* (Springer, New York, 1978).
- [36] R. Lehoucq, K. Machhoff, D. Sorensen, and C. Yang (www.caam.rice.edu/software/ARPACK).
- [37] J. K. Cullum and R. A. Willoughby, *Lanczos Algorithms for Large Symmetric Eigenvalue Computations* (Birkhauser, Boston, 1985).
- [38] E. R. Cohen and B. N. Taylor, *The 1986 Adjustment of the Fundamental Physical Constants*, report of the CODATA Task Group on Fundamental Constants, CODATA Bulletin 63, Pergamon, Elmsford, NY (1986); *Rev. Mod. Phys.* **57**, 1121 (1987).